ISSN (Print) 1226-1750
ISSN (Online) 2233-6656
Journal of Magnetics 17(4), 308-315 (2012) http://dx.doi.org/10.4283/JMAG.2012.17.4.308

Enhancement of the Magnetic Flux in Metglas/PZT-Magnetoelectric Integrated 2D Geomagnetic Device

D. T. Huong Giang, P. A. Duc, N. T. Ngoc, N. T. Hien, and N. H. Duc*

Department of Nano Magnetic Materials and Devices, Faculty of Engineering Physics and Nanotechnology, University of Engineering and Technology, Vietnam National University, Hanoi E3 Building, 144 Xuan Thuy Road, Cau Giay, Hanoi, Vietnam

(Received 9 November 2012, Received in final form 28 November 2012, Accepted 29 November 2012)

Experimental investigations of the magnetization, magnetostriction and magnetoelectric (ME) effects were performed on sandwich - type Metglas/PZT/Metglas laminate composites. The results have been analyzed by taking into account the demagnetization contribution. The study has pointed out that the magnetic flux concentration is strongly improved in piezomagnetic laminates with a narrower width leading to a significant enhancement of the ME effects. The piezomagnetic laminates with the optimal area dimension were integrated to form a 2-D geomagnetic device, which simultaneously can precisely detect the strength as well as inclination of the earth's magnetic field. In this case, a magnetic field resolution of better than 10^{-4} Oe and an angle precision of ± 0.1° were determined. This simple and low-cost geomagnetic-field device is promising for various applications.

Keywords : magnetoelectric effects, multiferroics, magnetic sensors, geomagnetic sensors, demagnetizing effects

1. Introduction

For the measurement of the terrestrial magnetic fields, magnetoelectric (ME) effect - based sensors have recently attracted much attention [1-6]. In comparison with the traditional types of magnetic sensors, which are based on fluxgate, Hall effects, superconducting quantum interference and giant magnetoresistance spin valves, *etc.* this generation of new magnetic sensor exhibits higher sensitivity to the intensity as well as to the direction of the geomagnetic field [1, 5]. Furthermore, this sensor shows additional advantages, such as simple and low-cost fabrication, and in particular, room-temperature operation. Regarding these advantages, multiphase laminated ME composites have been intensively studied [7]. Strong efforts have been undertaken to enhance the ME effects by altering the shape and the volume ratio of the piezoelectric/magnetostrictive laminates [8] or by improving the lamination process [9]. In such approaches, sandwich-type Metglas/PZT/Metglas laminate structures with long rectangular shapes, among others, have exhibited a huge magnetoelectric voltage coefficient (MEVC) of up to 22 V/cmOe [10]. Recently, we have achieved an enhancement of the *dc*-magnetic-field sensitivity of the ME sensor by using an elongated laminate shape [5]. This enhancement was thought to be related to the reduced demagnetization effects. Based on the results obtained from finite element modeling studies, Gao *et al.* [11], Cui *et al.* [12], Wu *et al.* [13] and Fang *et al.* [14] have ascribed the above-mentioned phenomena to the improved magnetic flux concentration in the ME laminates. These results have demonstrated a meaningful approach to significantly enhance the sensitivity of magnetostrictive/piezoelectric laminates as geomagnetic field sensors. However, more appropriate descriptions are still necessary in the models.

It is well known that both the strength and the inclination angle of the terrestrial magnetic field vary with the geographic positions on the Earth and in the space. Accordingly, appropriate geomagnetic-field sensors can be used in geographic orienting and positioning devices. The intention of our study is to develop this type of sensor for sensing and directing the relative orientation between a geostationary satellite and mobile transceivers in order to automatically control the mobile transceivers' antenna orientation with respect to the position of the geostationary satellite. This study is an approach toward improvement of the sensitivity to enable the ME device accurately determining the space azimuth (φ) and pitch

*Corresponding author: Tel: +84437547771
Fax: +84437547429, e-mail: ducnh@vnu.edu.vn

(θ) angles with respects to the orientation of the Earth's magnetic field.

In this paper, the introduction shall be followed by a lengthy magnetostatic analysis of the ME phenomena and the role of the piezomagnetic coefficient in Section 2, where the influence of the demagnetizing factor on the MEVC will be described and considered. Section 3 deals with the optimization of the low-field MEVC through experimental investigations of magnetization, magnetostriction and ME effects. A design and the characterization of the device prototype with a capability to detect both the azimuth and pitch angles of the geomagnetic field will be presented and discussed at the end of this section. Concluding remarks shall be given in Section 4.

2. Magnetostatic Analyses of the Size-Induced Demagnetization Effect on the MEVC

The ME effect has been observed in multiferroics and/or ferromagnetic-ferroelectric composites (hereafter denoted as ME materials). In these materials, a polarization P shall respond to an internal magnetic field H, whereas a magnetization M will respond to an internal electric field E. As a result, in applied magnetic fields, an ME sample shall undergo a polarization process that creates an electric field $E = \alpha_E \cdot H$ across the sample, where α_E ($=\partial E/\partial H$) denotes MEVC.

Considerable efforts have been undertaken to elaborate a phenomenological description of the MEVC ($\alpha_E = \partial E/\partial H$) [6, 11-17]. Although results are still diverse in details, the MEVC can generally be expressed as:

$$\alpha_E = \frac{dE}{dH} = \frac{\partial E}{\partial \lambda}\frac{\partial \lambda}{\partial H} \tag{1}$$

where λ represents the magnetostriction of the ferromagnetic phase and $\partial\lambda/\partial H$ is the so-called piezomagnetic coefficient of the material.

Taking into account the contribution of the demagnetizing factor (N) and M as the sample magnetization, the internal magnetic field can be expressed in term of the external magnetic field (H_0) as:

$$H = H_0 - NM \tag{2}$$

This leads to

$$H = \frac{H_0}{1 + N\chi_m} \tag{3}$$

with χ_m as the (intrinsic) magnetic susceptibility of the material.

Consequently, Eq. (1) becomes

$$\alpha_E = \frac{dE}{dH} = \frac{\partial E}{\partial \lambda}\frac{\partial \lambda}{\partial H_0}(1 + N\chi_m) \tag{4}$$

Finally, taking account the size-induced demagnetizing field's effect, the relative change in the MEVC of an ME laminate can be derived as follows

$$\frac{\alpha_E(N)}{\alpha_E(0)} = \frac{1}{1 + N\chi_m} \tag{5}$$

where $\alpha_E(0)$ and $\alpha_E(N)$ represent the intrinsic MEVC (as $N = 0$) and the extrinsic MEVC (as $N \neq 0$), respectively.

From Eq. (5), we can see that, the MEVC of an ME laminate composite is explicitly dependent on the (intrinsic) magnetic susceptibility (χ_m) and on the demagnetizing factor (N) of the magnetostrictive material. This implies that although the same magnetostrictive material is used, the MEVC still depends on the sample's shape. The sample with a large N, thus, will show a reduced the magnetic flux density over the central portion of the magnetic material and will exhibit a strongly reduced MEVC. This finding was recently reported by several research groups [11-14]. In ref. [13], a detail but rather complex dependence on the dimensions as well as the magnetic permeability was reported. Although a simpler expression could be found in [11], huge differences between the modeling and the experimental results still remained. As will be discussed below the present approach exhibits an appropriate consistence with experimental investigations.

3. Experimental Results and Discussion

3.1. ME laminate composite realization

The ME laminated composites for the magnetic-field sensors were manufactured by bonding an out-of-plane poled piezoelectric PZT plate with magnetostrictive Metglas laminates to form the sandwich Metglas/PZT/Metglas configuration (see Fig. 1). The 500 mm thick PZT plate used was of the Type APCC-855 from The American Piezoceramics Inc., PA, USA. The magnetostrictive laminates with thickness of 18 μm were cut from $Fe_{76.8}Ni_{1.2}B_{13.2}Si_{8.8}$ (also called Ni-based Metglas) melt-spun ribbons with different areas; the dimension of which is characterized by the length/width ratio r ($= L/W$). In this work, the sample's length was fixed at 15 mm and the width varies from 0.1 to 15 mm.

3.2. Magnetic data and analyses

Magnetization data were measured using a vibrating sample magnetometer in applied magnetic fields up to ± 300 Oe. For illustration, however, in Fig. 2(a) are plotted only the data measured in low magnetic-field range for

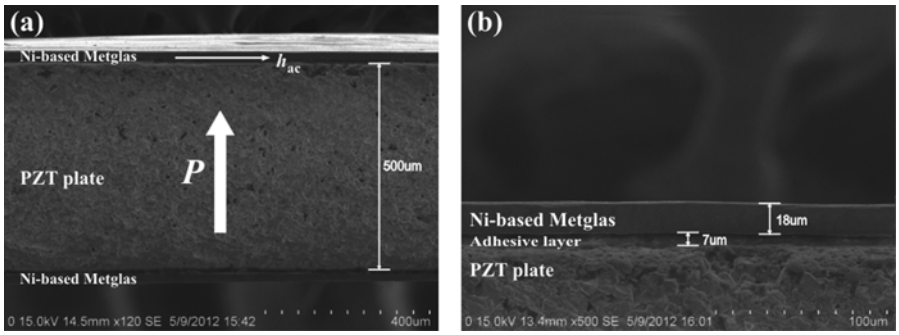

Fig. 1. SEM images at low (a) and high (b) magnification of the sandwich Metglas/PZT/Metglas laminate composite. Vectors h_{ac} and P indicate the applied *ac* magnetic field and the electrical polarization direction, respectively. In (b) the Metglas and the adhesive layer with the respective thickness of 18 μm and 7 μm are recognized.

the samples with the length/width ratio of r = 1, 15, 24, 40 and 140, where all samples noteworthy show the same saturation magnetization of 1950 emu/cm^3. Moreover, as can be seen from the figure, the low magnetic field magnetization slope strongly varies with r. This phenomenon is simply correlated with the sample's different demagnetizing factors N. The derived magnetic susceptibility data presented in Fig. 2(b) strongly confirm this argument. The Ni-based Metglas is already known as a super-soft magnetic material. For the longest sample under the present study (*i.e.* the sample with r = 140), the measured initial (extrinsic) magnetic susceptibility reached a value as high as χ_0 = 2326 emu, but we believe that this value is still far below the intrinsic one.

As will be shown below, the ME investigations were mainly focused on the samples with r = 1, 2, 3, 5, 7.5 and 15. The demagnetizing factor and its effect on the MEVC can be taken into account for by using the formula $N = 1/\chi_0 - 1/\chi_m$. For this range of r, one should realize that $1/\chi_m$ is (at least) about two order of magnitude smaller than $1/\chi_0$, so that it can be neglected in this consideration. Based on this assumption, the demagnetizing factor of a Metglas sample was derived from the measured values of the extrinsic magnetic susceptibility. The obtained results are presented in Fig. 3(a) as a plot of N_{exp} *vs* r. On the other hand, for comparison, the demagnetizing factor can also be directly calculated from the sample dimension parameters (*i.e.* its length, width and thickness) by using the software proposed in [18]. The calculated results are also shown in Fig. 3(d), again as a plot of N_{theory} *vs* r. As can be read from these results, the dimensions-based calculated N_{theory} value is almost three times larger than the experimentally derived N_{exp} one. Note that, the simulation on the relative change in the MEVC using Eq. (5) with N_{exp} shows a better consistency with the observed MEVC values than those with N_{theo}. This implies that an adequate theoretical approximation of the demagnetizating factor N for the thin square shaped samples still needs a more appropriate detailed description. Indeed, it was already warned in [19] that N is not a constant inside any magnetized sample that is not an ellipsoid and that a large disparity in different approximations of N is due to the square shape and small aspect ratio of thin samples.

Using the values as obtained for N in Eq. (5), the MEVC

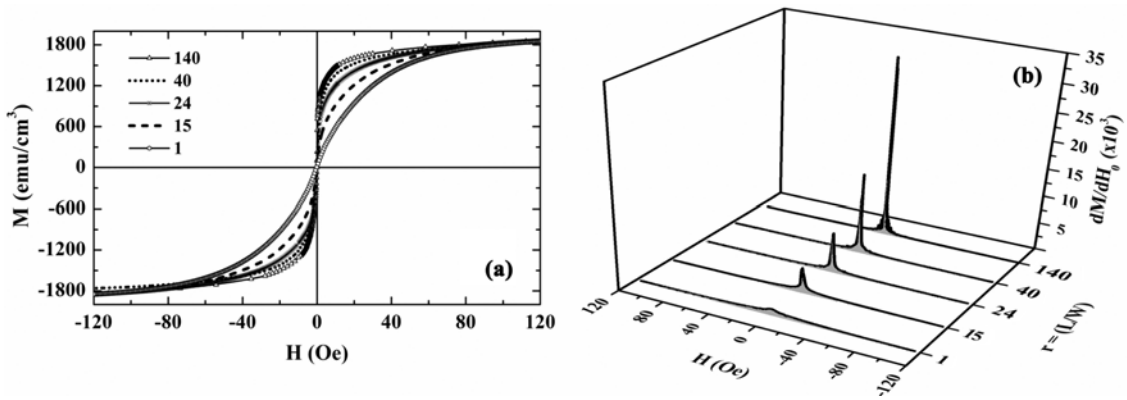

Fig. 2. Magnetization (a) and magnetic susceptibility (b) as a function of applied magnetic fields of ME laminates of different length/width ratios.

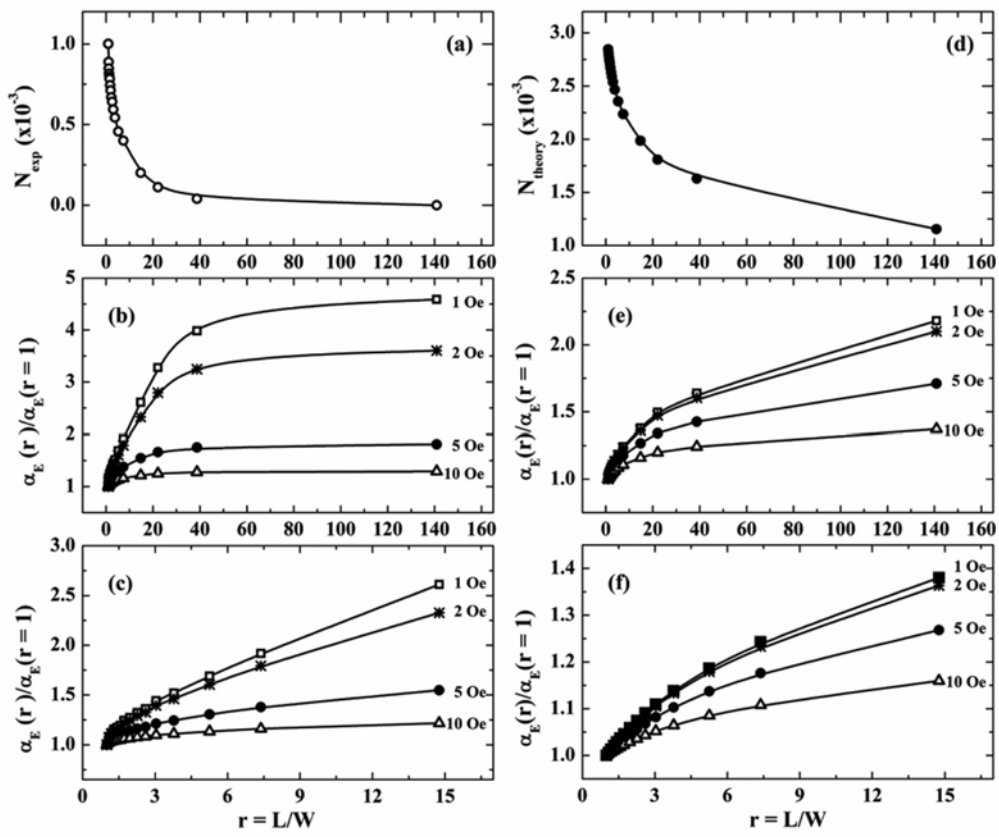

Fig. 3. Experimentally derived N_{exp} (a), calculated N_{theory} (d) demagnetization factors (see in the text) and corresponding normalized MEVC, calculated by using Eq. (5) as a function of the length/width ratio $r = L/W$ for all samples under investigations (b, e) and for samples under MEVC consideration only (c, f).

values, normalized to $\alpha_E(r)/\alpha_E(r = 1)$, in different applied magnetic fields of 1, 2, 5 and 10 Oe were determined. The results are shown in Figs. 3(b) and 3(e), corresponding to N_{exp} and N_{theory}, respectively. Note that, the results, also normalized to $\alpha_E(r)/\alpha_E(r = 1)$, from the simulation performed with the experimentally estimated values N_{exp} show a stronger variation than those from the simulation performed with the theoretically calculated N_{theory}. For instance, as the length/width ratio r increases from 1 to 15, the MEVC value at the field $H = 1$ Oe simulated using the demagnetizing factor N_{exp} is found to increase by 2.6 times, whereas that simulated using the N_{theory} yields an increase of 1.3 times only (see Figs. 3(e) and 3(f)). This finding is in reasonable consistency with the observed MEVC values presented in Subsection 3.4 below.

3.3. Magnetostriction and magnetostrictive susceptibility

Figure 4(a) shows the magnetostriction data in applied magnetic fields up to ± 120 Oe measured using an optical

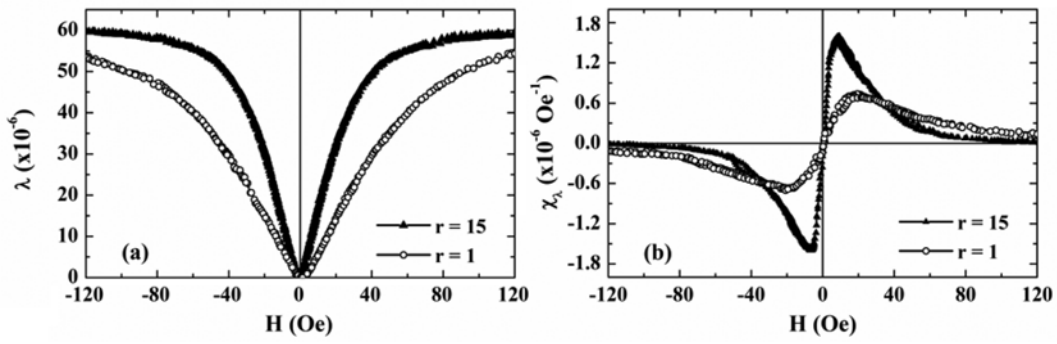

Fig. 4. Magnetostriction (a) and magnetostrictive susceptibility (b) data for samples with $r = 1$ and 15.

deflectometer for the two samples with r = 1 and 15, respectively. The magnetostriction reaches its saturation value of 60×10^{-6} in the sample with r = 15. Similar to magnetization data, the effect of the demagnetization is well demonstrated. Accordingly, the magnetostrictive susceptibility (or the piezomagnetic coefficient) χ_1 (= $\partial/\partial H_0$) was derived and presented in Fig. 4(b). Beside the information on the magnetoelastic properties of the ME samples, the results obtained directly indicate the size-induced demagnetization effect on the piezomagnetic coefficient. For the sample with r = 15, χ_1 initially increases rather fast in the low magnetic-field range and reaches the maximum at H_0 of about 9 Oe. For the sample with r = 1, however, χ_1 initially increases much slower, reaches the maximum only at about 20 Oe and slower decreases with further increasing field.

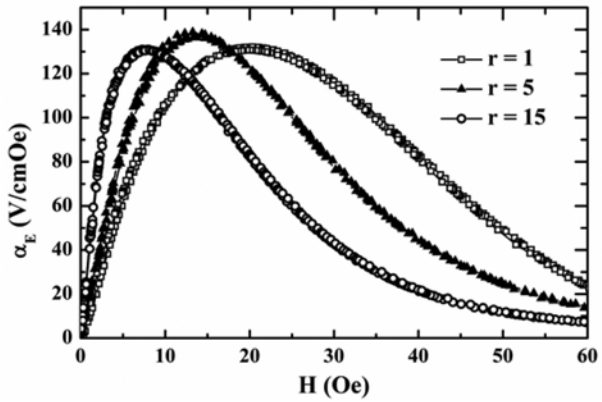

Fig. 5. MEVC as a function of the bias magnetic field for the sandwich Metglas/PZT/Metglas laminate composites with different r of 1, 5 and 15.

3.4. ME effects

In the ME laminate composites configuration as shown in Fig. 1, due to the mechanical coupling between the components, the PZT plate shall undergo a forced strain which is induced by the magnetostrictive layers under the in-plane applied magnetic field. The ME voltage response (MEVR) V_{ME} to this forced strain is subsequently induced across the thickness of the piezoelectric plate (t_{PZT}). In the present investigation, a linear electric polarization P is induced by a weak *ac* magnetic field h_{ac} (= $h_o \sin(2\pi f_o t)$) oscillating at the resonant frequency in the presence of a *dc* bias field H_0 and so the MEVR can be measured and considered as a direct response of the ME composite to the applied magnetic field. In the experimental setup, the bias field H_0 was provided by an electromagnet, and the oscillating field with amplitudes of $h_{ac} = 10^{-2}$ Oe was generated by a Helmholtz coil. The MEVR output induced across the PZT layer of the ME laminate by the *ac* field (h_{ac}) was measured on a commercial DSP lock-in amplifier (Model 7265, Signal Recovery), which simultaneously controlled the input current to the Helmholtz coil. The value of the MEVC (α_E) was then derived from the equation: $\alpha_E = V_{ME}/h_{ac}.t_{PZT}$.

Figure 5 shows the bias magnetic-field dependence of the longitudinal MEVC output measured at the resonant frequency (f_r = 99.6 kHz) for sandwich laminate composites of different sizes as 15 × 15, 15 × 3 and 15 × 1 mm^2, corresponding to the respective length/width ratios of r = 1, 5 and 15. As can be seen, for all samples the MEVC exhibits a similar behavior as already observed for the piezeomagnetic coefficient: it initially increases at low applied magnetic fields, reaches a maximum value at a certain magnetic field (denoted as the optimal field H_{max} for the maximal ME response) and then decreases with the further increasing magnetic field. It is apparent that although the maximal MEVC is significantly unchanged, the MEVC behavior is strongly influenced by the sample shape: the smaller the width (W), the lower the optimal magnetic field and the higher the initial slope at low magnetic fields is found for the MEVC α_E(H) curves. Indeed, the optimal magnetic field for the maximal ME response decreases from 21 Oe in the sample with r = 1 down to 7 Oe in the one with r = 15. Simultaneously, the initial slope at low magnetic fields of the $a_E(H)$ curves increases from 12.5 to 31.2 V/(cm·Oe^2), respectively.

The ME effect indeed is a multiple combination effect. The variation of α_E, in details, is interestingly not fully described by the piezomagnetic coefficient (χ_1) as expected. It is furthermore covered by the magnetoelastic energy (*i.e.* depending on λ), which is transferred from the magnetostrictive phase into the piezoelectric plate and by other piezoelectric parameters. The observed behavior of α_E (with respect to the bias magnetic field) follows rather well that of χ_λ, reflecting the fact that the piezomagnetic coefficient mainly governs the ME properties of the material.

Figs. 6(a, b) show the plots of $\alpha_E(r)$ and $\alpha_E(r)/\alpha_E(r = 1)$ as a function of r, representing the ME data measured in applied fields of 1, 2, 5 and 10 Oe in order to prove a possible correlation between the observed ME effect behavior and the role of the demagnetizing effect as already discussed above. Note that, the highest MEVC (α_E) was always reached in the sample with r = 15, *i.e.* the sample with the largest length to width ratio. Moreover, as the length to width ratio r of the ME laminates increases from 1 to 15, the observed MEVC is found to increase by 4.4, 3.4 and 0.2 times in the corresponding applied magnetic fields of 1, 2 and 10 Oe, respectively. This relative change is comparably consistent to that predicted from the magneto-

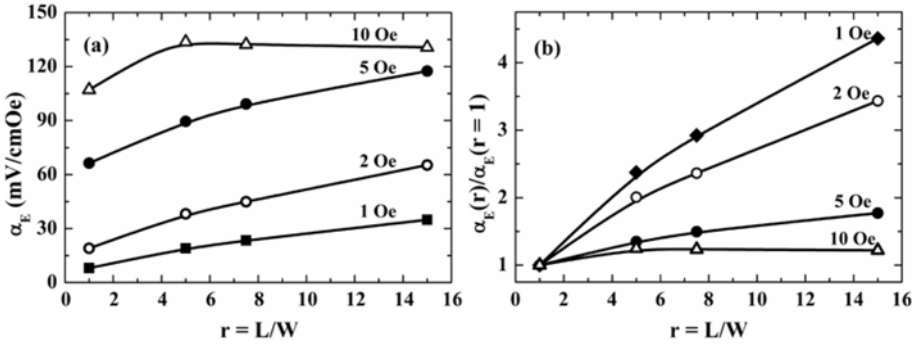

Fig. 6. Experimental data of MEVC (a) and normalized MEVC (b) as a function of the length/width ratio r at different H_{dc} of 1, 2, 5 and 10 Oe.

static analysis discussed above. Quantitatively, the relative increase in the observed MEVC found here is rather close to that obtained from the simulation performed with the experimentally estimated N_{exp} values (see *e.g.* Fig. 3(e) and Fig. 6(b)). Nevertheless, both the magnetostatic analysis and the experimental investigations have confirmed that the elongated Metglas shape plays a significant role on the enhancement of the magnetic flux concentration in ME laminate sensors. As regard the sensitivity to the magnetic field in the low field range, the sample with the configuration of 15 × 1 mm^2 obviously indicate to reach the optimization of all influencing factors. As a conclusion of this subsection, this 15 × 1 mm^2 laminate was chosen for a geomagnetic sensor prototype realization.

3.5. Geomagnetic sensor prototype

Regarding an appropriate application of the ME laminate composite configuration for the determination of the azimuth (φ) and the pitch (θ) angles with respect to the orientation of the Earth's magnetic field, the angle dependence of the MEVR is in close details studied. For this purpose, a functional 2-D ME sensor prototype was fabricated. In this case, firstly, a solenoid coil was directly wrapped around the ME laminate composites to form the 1-D sensor. The 2-D geomagnetic-field sensor is then created by assembling the two as-prepared 1-D sensors S_1 and S_2 along two orthogonal axes. The photograph of the 2-D sensor prototype fabricated using an ME laminates with optimal rectangular size of 15 × 1 mm^2 is shown in Fig. 7.

The MEVR characteristics of the S_1 and S_2 sensors are shown in Fig. 8. The figures obviously indicate a linear variation of ME-voltage with the external magnetic field in the field range of interest. From this result, it turns out that the magnetic field calibration coefficient k of the sensor can be derived as k_1 = 308.2 and k_2 = 310.7 mV/Oe corresponding to the field resolution of 3 × 10^{-4} Oe for the S_1 and S_2 sensors, respectively. This sensitivity is two

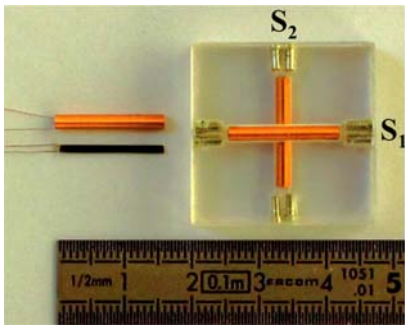

Fig. 7. (Color online) 1-D and 2-D ME sensor prototypes fabricated from sandwich Metglas/PZT/Metglas 15 × 1 mm^2 laminates composite.

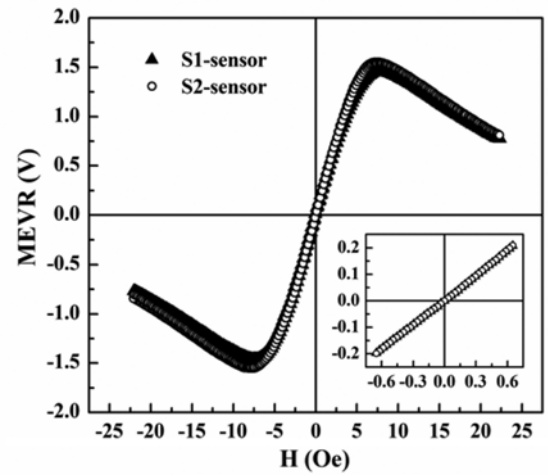

Fig. 8. The MEVR depending on the magnetic fields of the ME sensor prototypes. The inset shows the MEVR data at very small magnetic-field range.

orders of magnitude higher than that previously reported for similar magnetic-sensor devices and is comparable with that of available commercial geomagnetic sensors [20].

The horizontal component of the Earth's magnetic field strength is sensed by rotating the 2-D sensor in the Earth

surface's (horizontal) plane. A fixed geocentric reference frame is chosen, in which the X_E-axis points toward the magnetic North pole, the Y_E axis points toward the East pole and the Z_E-axis is vertical and positive towards the Earth's center (see Fig. 9(a)). Here, the azimuth angle is defined as a horizontal angle clockwise measured from X_E-axis to the S_1-sensor. The output offset-compensated signals V_1 and V_2 from the two respective sensors S_1 and S_2 as a function of the azimuth angle are plotted in Fig. 9(b-c). It is clearly seen that by rotating the device from φ = 0 to 360°, the recorded sensor signals vary well periodically with the angle φ, in which $V_1 = V_{1max}\cdot\cos\varphi$ and $V_2 = -V_{2max}\cdot\sin\varphi$ with V_{1max} = 123.2 mV and V_{2max} = 124.2 mV for the S_1 and S_2 sensors, respectively. The derived data for H_2 (= V_2/k_2) *vs* H_1 (= V_1/k_1) corresponding to the horizontal Earth's magnetic field components are plotted in the 2-D parametric plot (Fig. 9(c)) fitting a perfect circle. In this description, the radius of this circle, *i.e.* the intensity of the horizontal terrestrial magnetic-field components, can be determined using the following expression:

$$H_{xy} = \sqrt{(H_1^2 + H_2^2)} \tag{6}$$

It turns out in this experiment that the strength of the horizontal terrestrial magnetic-field H_{xy} in our laboratory (located in Hanoi, Vietnam) is in the order of 0.3997 Oe.

The pitch angle is determined as the angle between the S_1-sensor and the horizon by clockwise rotating the 2-D sensor around the X_E-axis, *i.e.* in the vertical planes as illustrated in Fig. 10(a). In this case, the obtained signals V_1 and V_2 from the two sensors S_1 and S_2 are shown in Fig. 10(b). They correspond well to the harmonic sine and cosine functions of the pitch angle θ. The maximum values of 61.4 and 61.9 mV for the sensors S_1 and S_2, respectively, were always reached when the sensor axis is pointing vertically upward (*i.e.* along the Z_E-axis).

The derived data on the intensity of the Earth magnetic-field components H_1 and H_2 presented in the 2-D para-

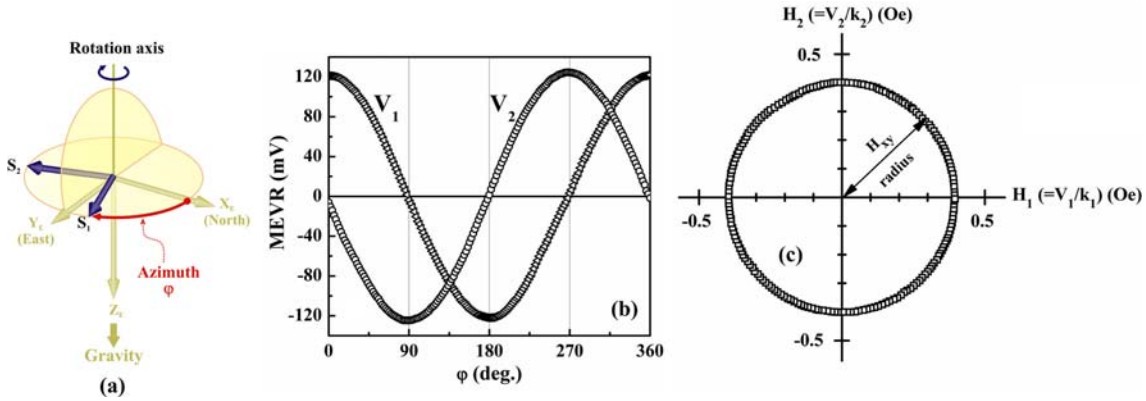

Fig. 9. (Color online) Illustration of the azimuth angle (φ) from the magnetic North pole (X_E-axis) to the S_1-sensor by rotating the 2-D sensor in a horizontal plane (a), MEVR of V_1 (open triangles) and V_2 (open circles) *vs* φ-angle, plotted in the Cartesian coordinate system (b) and the derived data for H_2 (= V_2/k_2) *vs* H_1 (= V_1/k_1), plotted in 2-D parametric plot.

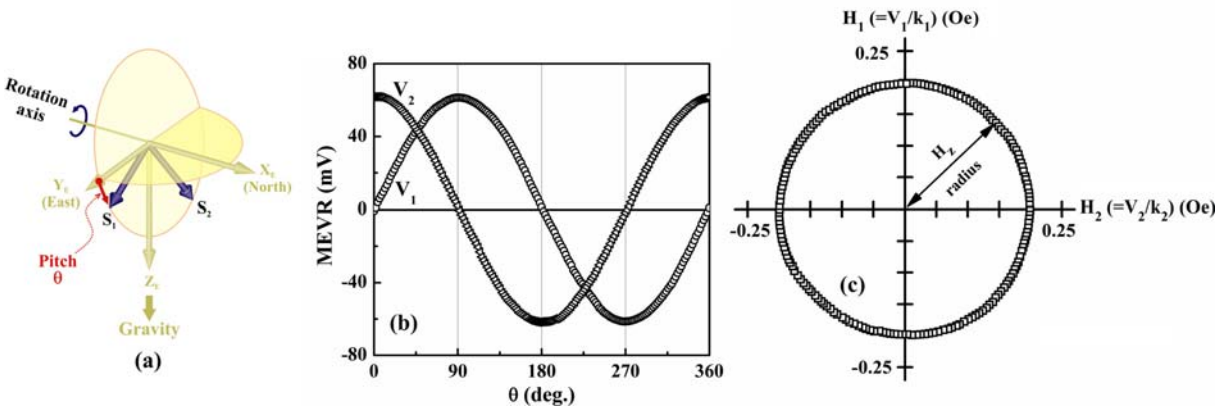

Fig. 10. (Color online) Illustration of the pitch angle between the S_1-sensor and the horizon plane in the clockwise rotation of the 2-D sensor around the X_E-axis (a), MEVR of V_1 and V_2 plotted in the Cartesian coordinate system (b) and the derived data H_1 (= V_1/k_1) *vs* H_2 (= V_2/k_2) plotted in 2-D parametric plot.

metric plot (see Fig. 10(c)) again fit in an almost perfect circle. From these data, the vertical terrestrial magnetic-field (H_z) component can be determined using the expression:

$$H_z = \sqrt{(H_1^2 + H_2^2)} \quad (6)$$

The calculation gives an accurate value of $H_z = 0.1992$ Oe. Combining with the above mentioned value of the horizontal component, the strength and inclination of the Earth's magnetic field in our laboratory were calculated to be 0.4466 Oe and 26°30', respectively. These findings are in good consistency with those reported previously [21, 22]. It suggests that the fabricated sensor can be used in any mobile device for a reliable detection of both the strength and the orientation of the geomagnetic field.

4. Concluding Remarks

An optimal giant magnetoelectric effect with a significant ME coefficient in the low magnetic field range has been reached on the basis of a simple, systematic magnetostatic analysis and of extended sophisticated experimental investigations taking into account the demagnetization effect. This study shows that the dimensional parameters (length and width) of the piezomagnetic laminates exert a strong effect on the magnetoelectric coupling: the narrower the laminate width, the higher the magnetic flux concentration in the ME laminates and the higher the MEVC. The study has provided a strong background supporting an optimal design of a terrestrial magnetic-field sensing device combining high performance Ni-based Metglas ribbons and poled piezoelectric PZT plates. The device as fabricated and tested can precisely detect not only the intensity, but also the azimuth and the pitch angle with respect to the orientation of the Earth's magnetic field. The sensibility and the resolution as achieved with respects to sensor fabrication make this device potential for application in novel smart compasses and positioning devices. In particular, this device also shows the capability to sense and distinct the relative orientation between a geostationary satellite and mobile transceivers and so providing the possibility to automatically determine and control the mobile transceiver's antenna direction with respect to the geostationary satellite position.

Acknowledgements

This work was supported by the NAFOSTED of Vietnam under the Research Project Number 103.02.86.09.

References

[1] J. Zhai, S. X. Dong, Z. Xing, J. Li, and D. Viehland, Appl. Phys. Lett. **91**, 123513 (2007).
[2] N. H. Duc and D. T. Huong Giang, J. Alloys Compd. **449**, 214 (2008).
[3] D. T. Huong Giang and N. H. Duc, Sens. Actuator A **149**, 229 (2009).
[4] L. Ding, J. Teng, X. C. Wang, C. Feng, Y. Jiang, G. H. Yu, S. G. Wang, and R. C. C. Ward, Appl. Phys. Lett. **96**, 052515 (2010).
[5] D. T. Huong Giang, P. A. Duc, N. T. Ngoc, and N. H. Duc, Sens. Actuator A **179**, 78 (2012).
[6] Y. Fetisov, A. Bush, K. Kamentsev, A. Ostashchenko, and G. Srinivasan, IEEE Sens. J. **6**, 935 (2006).
[7] C. W. Nan, M. I. Bichurin, S. Dong, D. Viehland, and G. Srinivasan, J. Appl. Phys. **103**, 031101 (2008).
[8] J. Blackburn, M. Vopsaroiu, and M. G. Cain, Adv. Appl. Ceram. **109**, 169 (2010).
[9] M. Li, D. Berry, J. Das, D. Gray, J. Li, and D. Viehland, J. Am. Ceram. Soc. **94**, 3738 (2011).
[10] S. X. Dong, J. Y. Zhai, J. F. Li, and D. Viehland, Appl. Phys. Lett. **89**, 252904 (2006).
[11] J. Gao, D. Gray, Y. Shen, J. Li, and D. Viehland, Appl. Phys. Lett. **99**, 153502 (2011).
[12] X. X. Cui and S. X. Dong, J. Appl. Phys. **109**, 083903 (2011).
[13] Z. Wu, Y. Wen, P. Li, J. Yang, and X. Dai, J. Magnetics **16**, 157 (2011).
[14] Z. Fang, S. G. Lu, F. Li, S. Datta, Q. M. Zhang, and M. E. Tahchi, Appl. Phys. Lett. **95**, 112903 (2009).
[15] Y. Fetisov, Y. K. Fetisov, and K. E. Kamentsev, Phys. Solid State **51**, 2308 (2009).
[16] G. Sreenivasulu, S. K. Mandal, S. Bandekar, V. M. Petrov, and G.. Srinivasan, Phys. Rev. B **84**, 144426 (2011).
[17] T. T. Nguyen, F. Bouillault, L. Daniel, and X. Mininger, J. Appl. Phys. **109**, 084904 (2011).
[18] http://www.magpar.net/static/magpar/doc/html/demag-calc.html
[19] R. C. O'Handley, Modern Magnetic Materials, John Wiley & Sons, New York (2000) p. 43.
[20] S. C. Mukhopadhyay and R. Y. M. Huang, Sensors, Springer-Verlag, Berlin-Heidelberg (2000) pp. 23-42.
[21] Ton Tich Ai, Geomagnetism and Magnetic Prospecting, Vietnam National University Publisher (2005).
[22] http://www.ngdc.noaa.gov/seg/geomag/jsp/struts/calcIGRFWMM.